general, the reaction diffusion bidomain solution yields a slightly broader biphasic deflection and slightly increased amplitude due to the transmural electrotonic effects of the bending wavefront. The results also show that the current source model is generally valid for the thick bath case, although the timecourse of the biphasic deflection coincident with activation is narrower than that predicted by either the full bidomain or analytical model, since all the sources are assumed to lie in an infinite volume conductor. The current source model, however, is not valid for the thin and no bath cases.

For tissue with a finite bath extent, the analytical model reveals that the extracellular potential, with a far field reference, can be interpreted of as being composed of the sum of two components; the particular (core-conductor) solution, and the homogeneous solution. The extent of the tissue and bath modulates the contribution these two solutions make to ϕ_e. As the bath becomes infinite, $b \to \infty$, $H_2(k) \to 0$, and the solution for ϕ_o and ϕ^h are simplified to the infinite bath derivation of Henriquez *et al.* [1]. As $b \to a$, the numerator of $H_3(k) \to 0$ and $\phi^h \to 0$. The solution for ϕ_e is, thus, the classical core-conductor equation [2]. Potentials from domains with bath thickness between these two extremes have contributions from both the particular and homogeneous solutions. For example, the potential on the tissue surface in the thin bath case (Fig. 2, site 3) is inverted and monophasic as predicted by the particular solution [see (3)] but with a smaller magnitude. This is due to the loading of the bath, through which current may be shunted. When no bath is present, the analytic and numerical solutions both reach the magnitude predicted by the particular solution.

A typical model to compute ϕ_e [see (15)] is based on the assumption that the transmembrane current sources lie in an extensive isotropic bath and, thus, resemble the thick bath case. Note that the impact of the bath depends on the tissue thickness and conductivities, as well as the conductivity of the bath and, therefore, the extensiveness of the bath cannot be determined from knowledge of bath thickness alone [8].

The analytic model is limited by the assumptions that $V_m(z)$ is constant in the depth (i.e., a planar front) and the tissue is equally anisotropic. As shown by Roth, an analogous set of equations can also be derived under the assumption that the intracellular potential is independent of depth (y-direction). This would allow for the tissue to have unequal anisotropy [8]. We expect the two models to have similar predictive power and computational costs.

In summary, the analytical model provides an efficient way to explore the extracellular potential in realistic bidomain preparations that involve a finite bath. In practice, $V_m(z)$ can be obtained from a monodomain model and the analytical model can then be used to estimate the extracellular potentials for tissue with a variably thick bath. The advantage of this approach is that the combined monodomain model and analytical model can be used to accurately solve for extracellular potentials in the presence of ionic inhomogeneities, while using considerably less computational time and resources than an equivalent bidomain.

REFERENCES

[1] C. Henriquez, N. Trayanova, and Plonsey, "A planar slab bidomain model for cardiac tissue," *Ann. Biomed. Eng.*, vol. 18, pp. 367–376, 1990.

[2] R. Plonsey, "Action potential sources and their volume conductor fields," *Proc IEEE*, vol. 65, pp. 601–611, 1977.

[3] C. S. Henriquez, "Simulating the electrical behavior of cardiac tissue using the bidomain model," *Crit. Rev. Biomed. Eng.*, vol. 21, pp. 1–77, 1993.

[4] M. Spach, W. Miller, E. Miller-Jones, R. Warren, and R. Barr, "Extracellular potentials related to intracellular action potentials during impulse conduction in anisotropic canine cardiac muscle," *Circ. Res.*, vol. 45, pp. 188–204, 1979.

[5] K. Gima and Y. Rudy, "Ionic current basis of electrocardiographic waveforms: A model study," *Circ. Res.*, vol. 90, pp. 889–96, 2002.

[6] R. Penland, D. Harrild, and C. Henriquez, "Modeling impulse propagation and extracellular potentials distribution in anisotropic cardiac tissue using a finite volume element discretization," *Comput. Vis. Sci.*, vol. 4, pp. 215–226, 2002.

[7] C. Luo and Y. Rudy, "A model of the ventricular cardiac action potential: Depolarization, repolarization," *Circ. Res.*, vol. 68, no. 6, pp. 1501–1526, 1991.

[8] B. J. Roth, "Effect of a perfusing bath on the rate of rise of an action potential propagating through a slab of cardiac tissue," *Ann. Biomed. Eng.*, vol. 24, pp. 639–46, 1996.

Correction of Motion Artifact in Cardiac Optical Mapping Using Image Registration

Gustavo K. Rohde*, Benoit M. Dawant, and Shien-Fong Lin

***Abstract*—Cardiac motion is one of the main sources of artifacts in epifluorescence imaging experiments. It can cause significant error in electrophysiological measurements such as action potential duration. We present a novel approach that uses image registration based on maximization of mutual information to correct for in-plane cardiac motion in such experiments. The approach is relatively fast (a few seconds per frame) and is performed entirely post acquisition. The image registration approach is an alternative to traditional approaches such as mechanical restraint of the heart or addition of chemical uncouplers. Our results show that the image registration method significantly reduces motion-related artifacts in experimental data.**

***Index Terms*—Image registration, motion correction, mutual information, optical mapping.**

I. INTRODUCTION

Optical recording techniques have been widely employed in cardiac electrophysiology for studies of electrodynamics. Optical mapping is based on the proportional change of the induced fluorescence intensity resulting from the change in the transmembrane potentials in dye-stained tissue. The most significant constraint in cardiac optical recording is muscle contraction, which alters the fluorescence intensity and deforms the shape of the optical potentials. When the tissue moves during the recording, its relative location to the sensor and the light source changes, resulting in an artificial variation of fluorescence intensity intermingled with the desired signal. Most significantly, quantification of intensity variation is not meaningful if the fluorescence is recorded from different sites on the tissue in the same recording

Manuscript received September 9, 2003; revised July 2, 2004. This work was supported in part by the National Institutes of Health (NIH) under Grant HL58533. *Asterisk indicates corresponding author.*

*G. K. Rohde is with the Applied Mathematics and Scientific Computation Program, University of Maryland, College Park, MD 20742-4015 USA (e-mail: rohdeg@math.umd.edu).

B. M. Dawant is with the Department of Electrical Engineering and Computer Science, Vanderbilt University, Nashville, TN 37235 USA (e-mail: benoit.dawant@vanderbilt.edu).

S.-F. Lin is with the Division of Cardiology, Department of Medicine, Cedars-Sinai Medical Center, Los Angels CA 90048 USA and also with the David Geffen School of Medicine, University of California at Los Angeles, Los Angeles CA 90048 USA (e-mail: linsf@cshs.org).

Digital Object Identifier 10.1109/TBME.2004.840464

episode. Tissue contraction starts immediately after the upstroke of action potential. Therefore motion artifacts are more pronounced during action potential plateau when contraction is maximal and during repolarization phase when relaxation occurs. As a consequence, the correct measurements of many interesting electrophysiological phenomena, such as action potential duration (APD) and repolarization, become impossible.

Common approaches to dealing with motion artifacts in fluorescence recording include mechanical constraining and chemical immobilization methods [1]–[4], which are applied prior to imaging. In this work, we instead propose a retrospective motion correction approach that is based on a post-processing software technique known as image registration to spatially align the sequence of digital images taken from the optical recorder such that each location in the images acquired represents an intensity measurement of the same tissue location throughout the recording episode. We have adapted an existing registration technique used in medical imaging (see Maintz *et al.* [5] for an overview of medical image registration) so as to suit the epicardial fluorescence imaging data.

II. Materials and Methods

A. Epifluorescence Mapping

The experimental procedure was similar to that of a previous study [4]. In brief, New Zealand white rabbits weighing 4.4–5.5 kg were injected with 1000 units of heparin and 70 mg/kg sodium pentobarbital to induce deep general anesthesia. The heart was excised and the ascending aorta cannulated and secured for retrograde perfusion of the coronaries with a modified HEPES perfusate. The potential-sensitive dye di-4-ANEPPS (Molecular Probes, OR) at a concentration of 0.5 μM was added to the perfusate for approximately 15 min to stain the heart. Fluorescence from the heart surface was elicited by a solid-state, frequency-doubled laser (Verdi V5, Coherent, Santa Clara, CA) at a wavelength of 532 nm. Laser light was delivered to the heart using multiple 1-mm optical fibers (SP-SF-960, FIS Inc., Oriskany, NY). The root-mean-square variation of laser intensity was 0.02%. The emitting fluorescence was imaged with a high-speed charge—soupled device camera (Model CA-D1-0128T, Dalsa Inc., Waterloo, ON, Canada) through a color glass filter with a cutoff wavelength of 600 nm (R60, Nikon).

B. Motion Correction via Image Registration

Given a series of N digital frames from the experimental setup described above $\{I_1(\mathbf{x}), I_2(\mathbf{x}), \ldots, I_N(\mathbf{x})\}$, where $\mathbf{x} = \{x, y\}$, we choose an image from the sequence that will serve as a reference frame for all other images. We call this reference frame $T(\mathbf{x})$. We then proceed to align each frame k in the original image sequence to the reference frame using the image registration algorithm proposed in [6], which finds the optimal alignment by solving numerically the following optimization problem:

$$\arg\max_{f_k} Q\left(I_k\left(f_k(\mathbf{x})\right), T(\mathbf{x})\right) \tag{1}$$

where $Q(.,.)$ is the mutual information image similarity measure and $f_k(\mathbf{x}) = A_k\mathbf{x} + \mathbf{t}_k$ is a two-dimensional affine spatial transformation containing six independent parameters capable of performing rotation, scaling, shear and translation, with $\mathbf{t}_k = \{(tx)_k, (ty)_k\}$. Maximization of mutual information was first proposed in medical image registration problems in [6], [7] and has been shown to be robust in matching images whose intensity values are not linearly related [8], [9].

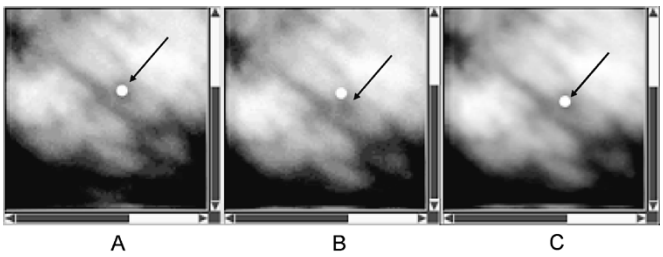

Fig. 1. Images from a movie sequence: (A) reference frame; (B) maximum displacement before motion correction; (C) maximum displacement after motion correction. The relative displacement between the marker (white dot), which is placed at the same exact coordinate in all images, and image features (pointed by black arrow) is visibly reduced after motion correction.

The mutual information similarity measure is given by

$$Q\left(I_k\left(f_k(\mathbf{x})\right), T(\mathbf{x})\right) = \sum_{i,t} p_{I_k,T}(i,t) \times \log\left(\frac{p_{I_k,T}(i,t)}{p_{I_k}(i)p_T(t)}\right) \tag{2}$$

where $p_{I_k}(i)$ and $p_T(t)$ are the marginal probability density functions (*pdf*) of $I_k(f_k(\mathbf{x}))$ and $T(\mathbf{x})$, respectively, and $p_{I_k,T}(i,t)$ is their joint *pdf*. The joint *pdf* $p_{I_k,T}(i,t)$ is computed from the normalized joint histogram of the images $I_k(f_k(\mathbf{x}))$ and $T(\mathbf{x})$ which is a matrix. The (i,t) entry of this matrix stores the number of pixels that have intensity i in image one and intensity t in image two. When divided by the total number of pixels, it is an estimate of the joint probability function of the intensity values of the two images. Marginal distributions are obtained by summing along the lines and columns of this matrix. In this work, we have used 64 bins (i.e., we have divided the intensity range into 64 intervals) to create the joint histograms. Note that indexes i, t, for which $p_{I_k}(i)$, $p_T(t)$ or $p_{I_k,T}(i,t)$ is zero are not included in the computation of (2). Given a transformation $f_k(\mathbf{x})$ the image $I_k(f_k(\mathbf{x}))$ is computed using bilinear interpolation.

As in [6], we use Powell's direction set method to compute the affine parameters that solve (1) [10]. Powell's direction set method requires only the evaluation of function values for optimizing a cost function. It goes about finding a minimum by using a set of conjugate, or "non-interfering," directions that are updated iteratively. For a quadratic cost function, it can be shown that Powell's method finds the minimum of the function in $M(M+1)$ line minimizations, where M is the number of parameters the cost function is dependent upon. The optimization is initialized with an identity transformation: all translation, rotation, and shear parameters set to zero, while the scaling parameters are set to 1. This ensures that $f_k(\mathbf{x}) = \mathbf{x}$. The tolerance value is 1.0e-4. Failure to increase the value of the similarity measure by more than 1.0e-4 in one optimization iteration signals completeness.

C. Data Analysis

Preliminary analysis of the data was done visually, focusing on regions of interest in which heart motion was evident. We analyzed the effect of our registration method on tissue activation quantitative measures such as action potential duration (APD), activation isochrones, as well as abnormal or excessive depolarization and repolarization extracted from the movie sequences. The tissue activation timing of each pixel is detected by the peak of the first derivative of the time variation of the recorded fluorescence intensity. Activation isochrones were constructed from all the activation timing in the entire image. The frame of tissue at diastole ($\boldsymbol{F_{rest}}$) was defined as the frame right before the activation wavefront entered the field of view, whereas the frame with peak transmembrane potential ($\boldsymbol{F_{peak}}$) was selected when the entire field was depolarized. Because the fluorescence intensity is

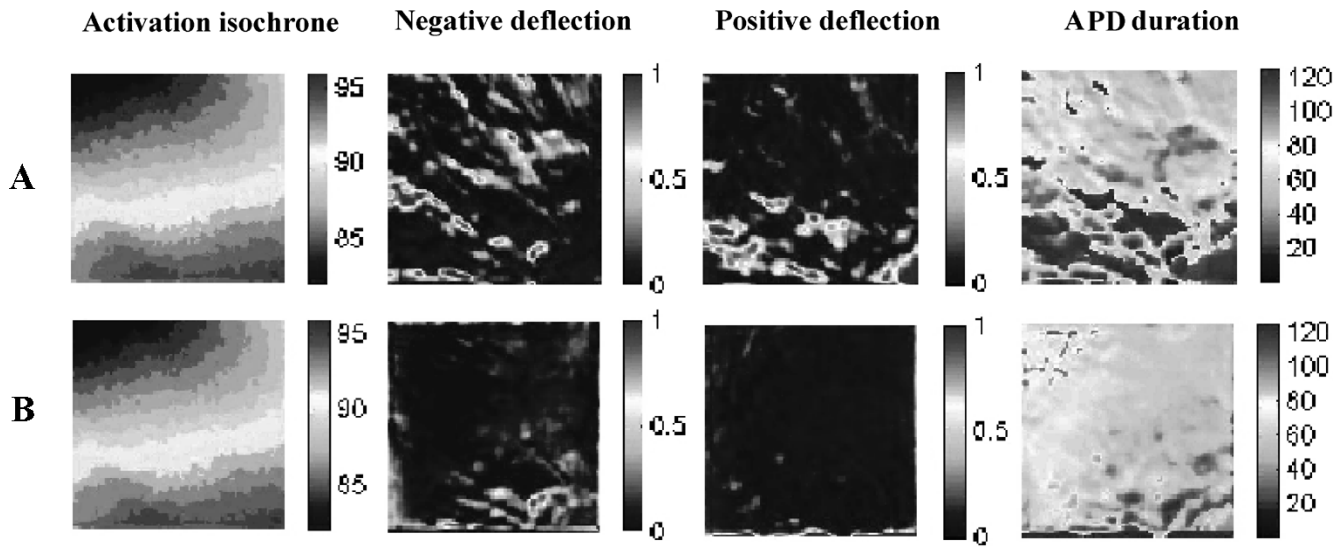

Fig. 2. Activation isochrones, negative and positive deflection, and activation potential duration (A) before and (B) after correction. Activation isochrones remain relatively intact after motion correction while positive and negative deflection artifacts are reduced. Activation potential duration measurements are also more uniform after motion correction.

negatively proportional to the amplitude of transmembrane potential, —($F_{peak} - F_{rest}$) represents the peak amplitude of the optical transmembrane potential (F_{amp}). For every pixel in the image sequence, the "excessive depolarization" was calculated from the maximum deviation from F_{peak} in the depolarized direction. Similarly, the "excessive repolarization" was calculated from the maximum deviation from F_{rest} in the repolarized direction. These two quantities were represented as a percentage of F_{amp} for all the pixels. The APD (APD50) was measured from the activation to the time when the amplitude fall below 50% of F_{amp} in the repolarizing phase. Lastly, positive and negative deflection artifacts are also visible in the individual traces (image intensity of a fixed pixel location over time) of the movies. We also include sample traces obtained before and after correction with our method.

III. Results

Fig. 1 displays representative registration results produced by the method described herein. Sequences of frames before [Fig. 1(A)] and after [Fig. 1(B)] registrations are shown. To help elucidate the motion present in the original sequence and the improvements in the corrected sequence we have placed a marker at the same pixel location for all frames. The reduced relative displacements between anatomical features and the marker after our motion correction approach indicate good overall alignment between the different movie frames. Fig. 2 shows the measured excessive repolarization (negative deflection) and excessive depolarization (positive deflection) before (row A) and after motion correction (row B). These effects have been greatly reduced after correction. The pattern of the activation potential wavefront propagation, as displayed by the movie's isochrones, remains intact. In addition, the APDs become significantly more evenly distributed after registration. Note that in this mode of motion, the tissue did not move out of the imaging field significantly. Fig. 3 shows two pairs of the original (top) and the corrected (bottom) traces. Pair A shows an upward deflection after the activation due to the motion, whereas pair B shows a downward deflection. Both these deflections are corrected using the image registration algorithm. Note that Figs. 1–3 show representative analyses results. The same experiment was conducted on a set of 11 movies. The results generated on these were similar to those presented here.

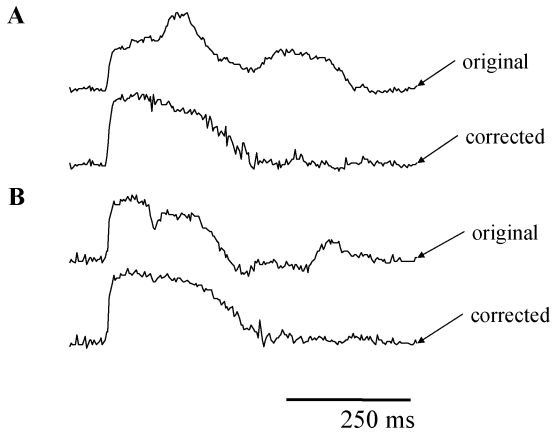

Fig. 3. Two examples of trace extracted from original and corrected movies. Deflection artifacts are visibly reduced after motion correction.

IV. Discussion and Conclusion

We have presented a simple method to correct for global motion present in epicardial fluorescence imaging experiments. Results showed that our approach significantly reduces motion artifacts of such image sequences. The algorithm is capable of reducing excessive depolarization and repolarization artifacts while preserving activation potential propagation. Activation potential duration is also more evenly distributed after correction with our approach. Our software was implemented in the IDL language (Research Systems, Inc.). The registration of each movie frame (128 × 128 pixels) takes about 5 seconds on a Pentium system running at 1.3 MHz. Implementing the software in a more efficient computer language such as C would certainly decrease computation time.

Note that the motion correction scheme presented here is one of many options. That is, instead of registering each movie frame to a single reference frame it is also possible to register each frame to the previous one. The advantage of the second approach is that the two consecutive frames should be more similar to each other. We have tried this option and, in our experience, this strategy is less stable than our current option. We have observed that while some corrections are good, some experiments generated results that were noticeably incorrect. We

believe that the cause for this is the accumulation of successive registration errors. That is, the error for the registration of say frames 0 and 1 may be small, and so may be the error in the registration of frames 1 and 2. The error for the registration of frames 0 and 2, however, should in theory be larger than the error between 0 and 1 or the error between 1 and 2. Since the movie sequences we are using contain hundreds of frames, it is easy to see how this strategy can potentially generate highly inaccurate results. Yet another option is to use a single reference frame and initialize the optimization procedure using the result of the registration of the previous frame. We are currently investigating such options and trying to improve the quality of our corrections.

It is important to clarify the limitations of our approach. First, all motions are assumed to be in plane. Thus out of plane motions cannot be corrected and in some instances may confound our correction approach. Furthermore, pixels that moved out of the imaging field due to motion cannot be recovered. Possible solutions to both problems include imaging the surface of the heart in stereo with multiple cameras or mirrors. This would allow collection of three-dimensional information that could be used to correct for motion artifacts out of the imaging plane. In addition, we only corrected for global motions (rotations, translations, shear and scaling) in this initial attempt to use image registration to correct for motion artifacts. Local motions can be further corrected using nonrigid (nonlinear) registration methods. Preliminary results indicate that this is a promising direction, though technical implementation details can be complicated.

In our experience we have found that the method presented above works best with images that have a small field of view focused on the surface of the heart. This could be related to the fact that while the affine spatial transformation model we use may be appropriate to describe local movement, it is not an appropriate model to simultaneously describe movement of several regions of the heart. The images presented in this paper have a field of view of about 20×20 mm, with resolution of about 200×200 microns.

In addition, it should also be noted that the method described above may fail to correct for motion in image sequences that have a large activation signal to noise ratio. In such cases, the algorithm may confound image features with activation signal, making motion correction difficult. The activation signal to noise ratio for our images falls typically in the 5 to 10 range. Initial experiments show that the algorithm works well for such images. At this point, however, we have not performed experiments to determine exactly at which activation signal to noise the algorithm starts failing.

REFERENCES

[1] I. R. Efimov, D. T. Huang, J. M. Rendt, and G. Salama, "Optical mapping of repolarization and refractoriness from intact hearts," *Circulation*, vol. 90, pp. 1469–1479, 1994.

[2] K. F. Kwaku and S. M. Dillon, "Shock-induced depolarization of refractory myocardium prevents wave-front propagation in defibrillation," *Circ. Res.*, vol. 79, pp. 957–973, 1996.

[3] R. A. Gray, A. M. Pertsov, and J. Jalife, "Spatial and temporal organization during cardiac fibrillation," *Nature*, vol. 392, pp. 75–78, 1998.

[4] S. F. Lin, B. J. Roth, and J. P. Wikswo, Jr., "Quatrefoil reentry in myocardium: an optical imaging study of the induction mechanism," *J. Cardiovasc. Electrophysiol.*, vol. 10, pp. 574–586, 1999.

[5] J. B. Maintz and M. A. Viergever, "A survey of medical image registration," *Med. Image Anal.*, vol. 2, pp. 1–36, 1998.

[6] F. Maes, A. Collignon, D. Vandermeulen, G. Marchal, and P. Suetens, "Multimodality image registration by maximization of mutual information," *IEEE Trans. Med. Imag.*, vol. 16, no. 2, pp. 187–198, Apr. 1997.

[7] W. M. Wells 3rd, P. Viola, H. Atsumi, S. Nakajima, and R. Kikinis, "Multi-modal volume registration by maximization of mutual information," *Med. Image Anal.*, vol. 1, pp. 35–51, 1996.

[8] C. Studholme, D. L. Hill, and D. J. Hawkes, "Automated three-dimensional registration of magnetic resonance and positron emission tomography brain images by multiresolution optimization of voxel similarity measures," *Med. Phys.*, vol. 24, pp. 25–35, 1997.

[9] J. West, J. M. Fitzpatrick, M. Y. Wang, B. M. Dawant, C. R. Maurer Jr., R. M. Kessler, R. J. Maciunas, C. Barillot, D. Lemoine, A. Collignon, F. Maes, P. Suetens, D. Vandermeulen, P. A. van den Elsen, S. Napel, T. S. Sumanaweera, B. Harkness, P. F. Hemler, D. L. Hill, D. J. Hawkes, C. Studholme, J. B. Maintz, M. A. Viergever, G. Malandain, and R. P. Woods *et al.*, "Comparison and evaluation of retrospective intermodality brain image registration techniques," *J. Comput. Assist. Tomogr.*, vol. 21, pp. 554–566, 1997.

[10] W. H. Press, S. A. Teukolsky, W. T. Vetterling, and B. P. Flannery, *Numerical Recipes in C: The Art of Scientific Computing*. Cambridge, U.K.: Cambridge Univ. Press, 1992.